ELSEVIER

www.elsevier.nl/locate/jorganchem

Journal of Organometallic Chemistry 609 (2000) 66–76

Journal of Organometallic Chemistry

Photodissociation and electronic spectroscopy of transition metal hydrides carbonyls: quantum chemistry and wave packet dynamics

Marie Catherine Heitz [1], Dominique Guillaumont, Isabelle Cote-Bruand, Chantal Daniel *

Laboratoire de Chimie Quantique, UMR 7551 CNRS/Université Louis Pasteur, 4 Rue Blaise Pascal 67 000 Strasbourg, France

Received 15 June 2000

Abstract

The photodissociation mechanism of a number of transition metal carbonyl hydrides ($HCo(CO)_4$, $H_2Fe(CO)_4$, $HM(CO)_3$(H-DAB) with M = Mn, Re and H-DAB = 1,4-diaza-1,3-butadiene) is followed in a time-dependent approach. The time scale of the primary reactions, the absorption spectra and the branching ratio of the concurrent dissociation pathways are deduced from wave packet propagations performed on two-dimensional ab initio potential energy surfaces connecting the electronic ground and excited states of the irradiated molecule to those of the primary products. © 2000 Elsevier Science S.A. All rights reserved.

Keywords: Electronic spectroscopy–photoreactivity; Transition metal hydrides carbonyls; Quantum chemistry; Wavepacket dynamics

1. Introduction

Transition metal hydride complexes undergo a variety of photochemical reactions with experimental evidence obtained for both homolysis of the metal–hydrogen bond [1] and the ligand dissociation [2], the latter being the major process in carbonyl compounds. Evidence was reported that elimination of H_2 is likely upon photolysis of dihydrides and polyhydrides leading to highly reactive intermediates able to activate the carbon–hydrogen bonds in saturated organic compounds [3]. Production of catalytically active species, synthesis of substituted derivatives, initiation of polymerization or spectroscopic investigation of short-lived intermediates are among the wide variety of applications connected to this field.

Although theoretical studies of the photoreactivity of transition metal complexes were not common before 1985, several qualitative aspects of their photoreactivity began to emerge in the late 1980's based on state correlation diagrams and potential energy curves [4–6]. It has been shown that the homolysis of the metal–hydrogen bond in monohydrides is a rather general reaction, although it may be obscured in some systems by the competition with the photodissociation of other ligands. The general occurrence of the homolysis of the M–H bond and the elimination of H_2 upon irradiation of transition metal mono and dihydrides, respectively, is not fortuitous. Indeed, the metal–hydrogen bond breaking results from the dissociative character of the potential energy curve associated to the triplet excited state corresponding to the $\sigma_{M-H} \rightarrow \sigma^*_{M-H}$ excitation and leading to the formation of radicals. Also the elimination of H_2 is a consequence of the dissociative character of the potential energy curves associated to the states resulting from a one-electron excitation from a metal–H_2 bonding orbital to a metal–H_2 antibonding orbital. For the first time a distinction was made between the photoactive excited state initially populated after irradiation and the state responsible for the observed primary process. These qualitative mechanisms have been extended to a variety of molecules that upon irradiation, either at a unique wavelength or at different wavelengths, undergo concurrent photochemical reactions like metal–alkyl or metal–metal bonds breaking versus ligand dissociation. The aim of this pioneering work was to interpret conventional experiments using non selective irradiation and characterized by poorly resolved absorption spectra.

* Corresponding author. Tel.: +33-3-88416076; fax: +33-3-88612085.

E-mail address: daniel@quantix.u-strasbg.fr (C. Daniel).

[1] Present address: Laboratoire de Physique Quantique, UMR 5626 IRSAMC Université Paul Sabatier, Toulouse, France.

PII: S0022-328X(00)00385-5

More quantitative information about the photodissociation mechanism requires the detailed knowledge of potential energy surfaces associated with the low-lying excited states participating in the photoreactivity, coupled with a dynamical study of the primary reactions. For this purpose accurate quantum chemical calculations of the excited states potential energy surfaces have to be performed and the elementary processes (intramolecular vibrational energy redistribution, intersystem crossing, internal conversion, direct dissociation, indirect dissociation via tunneling) have to be considered under a time-dependent approach. The development of highly correlated methods (CASSCF, MR-CCI, CASPT2) adapted to the handling of the electronic problem in middle size transition metal complexes (10 to 20 atoms) and the increase of computer facilities has enabled us to propose reasonable two-dimensional potential energy surfaces describing the competition between two potentially reactive channels for a number of transition metal hydrides since the early 1990's [7,8].

Although the field of molecular photodissociation dynamics has been expanded tremendously during the last decade [9] and applied with success to small systems [10], the application of quantum time-dependent wave packet propagation method to multi-dimensional systems has to be driven with care under certain approximations. The main problem is related to the reduction of dimensionality which cannot be applied a priori. Fortunately, transition metal complexes are less flexible than small organic molecules and in a first approximation the system does not undergo important geometrical deformations (except the ones corresponding to the reaction pathways) in the excited states directly accessible through vertical excitation (Franck–Condon). Moreover, the time scale of direct dissociation range between 20 to 200 fs [11] which excludes a complete relaxation of the molecule during such an ultra-fast process.

Ideally the theoretical investigations should be coupled to femtosecond laser pump and probe experiments [12,13]. If these techniques have been tentatively applied to a few transition metal carbonyls [14–17] with a lot of difficulties (coherent control, excess of energy, photofragmentation) they have never been applied to transition metal hydrides. As a consequence the theoretical simulation precedes the experiments.

In this short review four systems are presented (Scheme 1): two real systems $HCo(CO)_4$ and $H_2Fe(CO)_4$ representative of mono and dihydride com-plexes, respectively and two model systems $HMn(CO)_3$(H-DAB) and $HRe(CO)_3$(H-DAB) which possess the fascinating photoreactivity of Metal-to-Ligand-Charge-Transfer (so-called MLCT) complexes $LM(CO)_3$(H-DAB) (L = alkyl, halide, metal) [18]. Indeed upon visible irradiation these molecules undergo either CO loss to lead to the

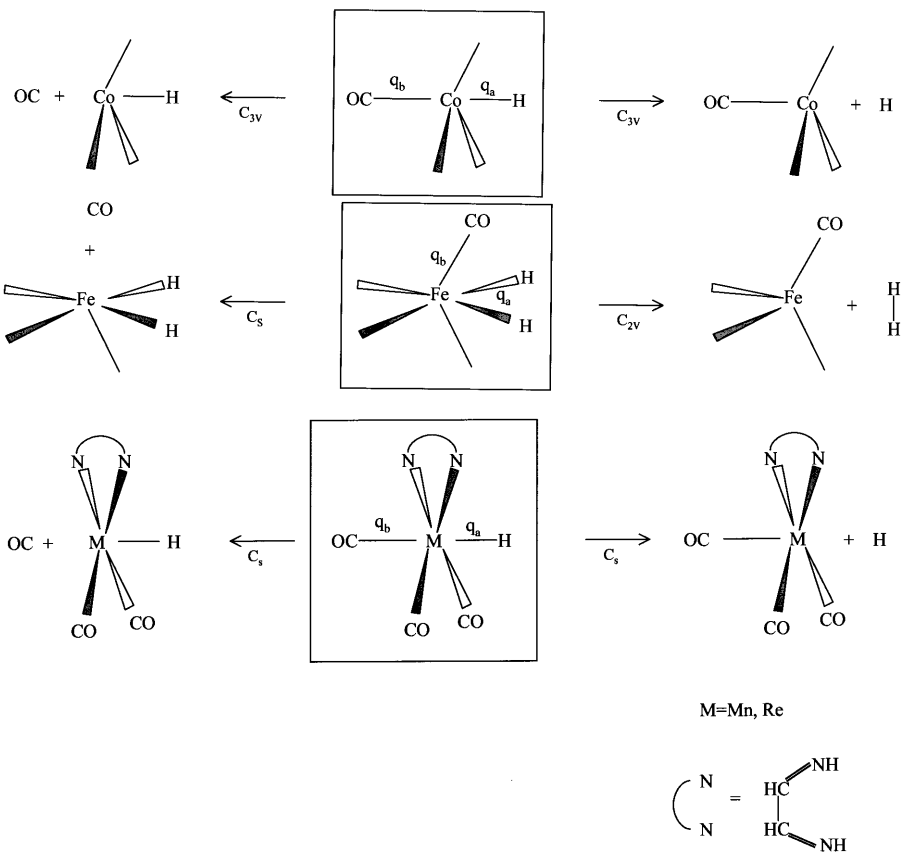

Scheme 1.

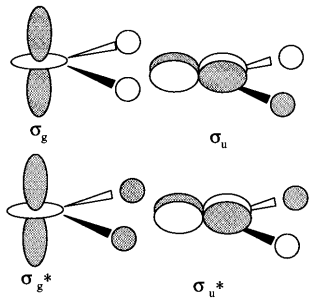

Scheme 2.

formation of unsaturated fragments $LM(CO)_2$(H-DAB) or homolysis of the metal–L bond to form radicals $^{\bullet}M(CO)_3$(H-DAB), a third channel of deactivation being emission from a long life time excited states [$LM(CO)_3$(H-DAB)]* precursor of electron and energy transfer processes. The quantum yield of the different photoproducts depends on the metal center, on the α-diimine ligand and on the ligand L.

A brief summary of the computational methods is reported in Section 2. The next section is devoted to the photodissociation dynamics of the molecular systems represented in Scheme 1 with a short recall of the experimental findings. Concluding remarks and perspective are presented in the last section.

2. Computational methods

2.1. Quantum chemistry

Since we are interested by fast events (vertical transitions in the Franck–Condon domain, direct dissociations occurring in the femtosecond time scale and intersystem crossings occurring in the picosecond time scale) a systematic geometry optimization of the excited states is not performed a priori. In any cases, the geometrical deformations when going from the equilibrium to the dissociated fragments are not sufficiently significant to justify costly gradient calculations at a correlated level. In order to study the molecular deformation of the molecule in the low-lying excited states, especially in MLCT complexes which possess quasi-bound states, a few gradient/CASSCF optimizations have been performed on $HM(CO)_3$(H-DAB) (M = Mn, Re) [19]. It has been shown that the most affected geometrical parameters when going from the electronic ground state to the low-lying excited states are the M–H and M–CO_{ax} bonds, the other ligands playing a role of 'spectators' at first glance. Most of the time geometry optimizations attempted on transition metal carbonyls fail because of the presence of excited states with accentuated dissociative character for one or several degrees of freedom.

It has been assumed that the C_{3v} symmetry is retained along the reaction path describing the photochemistry of $HCo(CO)_4$ (Scheme 1). The C_{2v} symmetry has been conserved along the reaction path corresponding to the H_2 photoelimination of $H_2Fe(CO)_4$ whereas the CO loss has been described under the C_s symmetry constraint. The C_s symmetry constraint has also been used for the investigation of the two primary reactions describing the photoreactivity of $HM(CO)_3$(H-DAB) (M = Mn, R).

Excited states calculations are based on MR-CCI methods performed on CASSCF wavefunctions averaged over the low-lying states of a given spin and symmetry and including the molecular orbitals involved in the excited states participating to the photoreactivity of the molecule under investigation. This set of molecular orbitals consists of the 3d (first row transition metal hydrides) or 5d (third row transition metal hydrides) occupied and vacant orbitals, the 3d′ and 5d′ which correlate them, the σ_{M-H} and σ^*_{M-H} orbitals which are metal–hydrogen bonding and anti-bonding, respectively (in the mono-hydrides), and the σ_g, σ^*_g, σ_u and σ^*_u orbitals which are either H–H bonding and metal–H_2 bonding (σ_g) and anti-bonding (σ^*_g) or H–H anti-bonding and metal–H_2 bonding (σ_u) and anti-bonding (σ^*_u) (in the dihydrides) (Scheme 2).

The low-lying $\pi^*_{H\text{-}DAB}$ orbitals localized on the α-diimine acceptor ligand of the MLCT complexes $HM(CO)_3$(H-DAB) are added in the CASSCF active space. The number of correlated electrons ranges between eight and ten. The computational details concerning the basis sets, the MR-CCI calculations, the kinetic and spin–orbit couplings and the software used are described elsewhere, as well as the MR-CCI results validation by CASPT2 calculations [20–23].

2.2. Wave packet dynamics

The photoabsorption and the subsequent bonds breaking described in Scheme 1 are simulated by propagation of selected wave packets $\Psi_e(q_a, q_b, t)$ on the two-dimensional potentials $V_e(q_a, q_b)$ corresponding to the electronic excited states e and calculated as a function of the two coordinates $q_a = [M - H]$ ($HCo(CO)_4$ and $HM(CO)_3$(H-DAB)) or $[M - H_2]$ ($H_2Fe(CO)_4$) and $q_b = [M - CO]$. The time evolution of the wave packets is obtained by solving the time-dependent Schrödinger equation:

$$i\hbar \frac{\partial}{\partial t} \Psi_e(q_a, q_b, t) = [T_{nu} + V_e]\Psi_e(q_a, q_b, t) \quad (1)$$

with the following initial conditions

$$\Psi_e(q_a, q_b, t = 0) = \mu_e \Phi_{gs,0}(q_a, q_b) \quad (2)$$

where μ_e is the electronic transition moment between the electronic ground state (gs) and the excited state e. $\Phi_{gs,0}(q_a, q_b)$ represents the two-dimensional vibrational ground wavefunction of the electronic ground state evaluated either through the coupled Morse oscillators method [24] or through the Chebychev relaxation

method [25]. The solution of the time-dependent Schrödinger Eq. (1) is obtained either by the second-order-differential propagation scheme [26] or by the Chebychev propagation method [27].

The Fourier Transform of the total autocorrelation function $S_{tot}(t)$ gives the absorption spectrum σ_{tot}

$$\sigma_{tot}(\omega) \propto \omega \int_{-\infty}^{+\infty} dt\ e^{i(E_i+\omega)t} S_{tot}(t) \quad (3)$$

where

$$S_{tot}(t) = \sum_e \langle \Psi(0) | \Psi(t) \rangle \quad (4)$$

and E_i represents the energy of the initial wave packet on the electronic state e.

The kinetic part of the Hamiltonian of the system, expressed in bond coordinates, is given by

$$T_{nu} = -\frac{\hbar^2}{2\mu_a}\frac{\partial^2}{\partial q_a^2} - \frac{\hbar^2}{2\mu_b}\frac{\partial^2}{\partial q_b^2} + \frac{\hbar^2}{m_c}\frac{\cos\theta\ \partial^2}{\partial q_a\ \partial q_b} \quad (5)$$

where μ_a and μ_b are the reduced masses corresponding to the bonds q_a and q_b and m_c is the mass of the central atom. Reaction probabilities are deduced by integration, over the whole reaction time, of the probability current density expressed as a function of coordinates q_a and q_b [28] (with θ kept constant to 180.0° for $HCo(CO)_4$ and $HM(CO)_3$(H-DAB), M = Mn, Re and θ kept constant to its experimental value of 74.25° for $H_2Fe(CO)_4$) (Scheme 1),

$$\vec{J}(q_a, q_b, t) = \begin{pmatrix} J_a(q_a, q_b, t) \\ J_b(q_a, q_b, t) \end{pmatrix} \quad (6)$$

where

$$J_a(q_a, q_b, t) = \frac{1}{\mu_a} \mathrm{Re}\left(\Psi^*(q_a, q_b, t) \frac{\hbar}{i} \frac{\partial}{\partial q_a} \Psi(q_a, q_b, t) \right) + \frac{\cos\theta}{m_c} \mathrm{Re}\left(\Psi^*(q_a, q_b, t) \frac{\hbar}{i} \frac{\partial}{\partial q_b}(q_a, q_b, t) \right) \quad (7)$$

and $J_b(q_a, q_b, t)$ being defined in the symmetric way.

3. Results

3.1. Photodissociation dynamics of $HCo(CO)_4$: prototype for first-row transition metal mono-hydrides [21,22]

The photodissociation of $HCo(CO)_4$

$$HCo(CO)_4 \xrightarrow{h\nu} H + Co(CO)_4 \quad (R1)$$

$$HCo(CO)_4 \xrightarrow{h\nu} CO + HCo(CO)_3 \quad (R2)$$

is described by wave packet propagation on the spin–orbit coupled two-dimensional CASSCF/MR-CCI Potential Energy Surfaces (PES) calculated along the two reaction coordinates q_a = [Co–H] and q_b = [Co–CO_{ax}] for the ^1E ($3d_\delta \rightarrow \sigma^*_{Co-H}$), ^3E ($3d_\delta \rightarrow \sigma^*_{Co-H}$) and $^3A_1$ ($\sigma_{Co-H} \rightarrow \sigma^*_{Co-H}$) excited states. Both reactions have been observed in low-temperature matrices [29] with the second reaction (R2) being the major process under these particular experimental conditions.

Table 1
CASSCF/MR-CCI excitations energies (cm^{-1}) to the low-lying excited states of $HCo(CO)_4$

Transition	One-electron excitation in the principal configuration	CASSCF/MR-CCI
$a^1A_1 \rightarrow {}^1E$	$3d_\delta \rightarrow \sigma^*_{Co-H}$	36 000
$a^1A_1 \rightarrow {}^3E$	$3d_\delta \rightarrow \sigma^*_{Co-H}$	25 900
$a^1A_1 \rightarrow {}^3A_1$	$\sigma_{Co-H} \rightarrow \sigma^*_{Co-H}$	34 600

The CASSCF/MR-CCI excitation energies are reported in Table 1. According to the experiments, the photoreactivity (R1, R2) occurs after irradiation at 254 nm (39 370 cm^{-1}) and the absorption starts at 285 nm (35 000 cm^{-1}) with a maximum around 227 nm (44 000 cm^{-1}). The ^1E excited state seems to be a good candidate for a direct absorption in the UV energy domain.

The molecular reaction dynamics of competitive direct dissociation of $HCo(CO)_4$ via the ^1E excited state versus the indirect spin–orbit induced dissociation via the $^3A_1$ and ^3E excited states, illustrated in Fig. 1, have been obtained by solving a set of coupled time-dependent Schrödinger equations (where ^3X represents either the $^3A_1$ or the ^3E state) in the diabatic representation [21,22,30]

$$i\hbar \frac{\partial}{\partial t} \Psi_{^1E}(q_a, q_b, t) = [T_{nu} + V_{^1E}]\Psi_{^1E}(q_a, q_b, t) + V_{^1E^3X}\Psi_{^3X}(q_a, q_b, t) \quad (8a)$$

$$i\hbar \frac{\partial}{\partial t} \Psi_{^3X}(q_a, q_b, t) = [T_{nu} + V_{^3X}]\Psi_{^3X}(q_a, q_b, t) + V_{^3X^1E}\Psi_{^1E}(q_a, q_b, t) \quad (8b)$$

with the following initial conditions

$$\Psi_{^1E}(q_a, q_b, t = 0) = \mu_{^1A_1 \rightarrow {}^1E}\Phi_{^1A_1,0,0}(q_a, q_b) \quad (9a)$$

$$\Psi_{^3X}(q_a, q_b, t = 0) = 0 \quad (9b)$$

and constant values of 25 and 335 cm^{-1} for the spin–orbit coupling potentials $V_{^1E^3A_1}$ and $V_{^1E^3E}$, respectively as estimated from [31].

The time evolution of representative wave packets $\Psi_{^1E}(q_a, q_b, t)$ and $\Psi_{^3A_1}(q_a, q_b, t)$ on the coupled PES is depicted in left side of Fig. 1(A) and right side of Fig. 1(A), respectively. According to the initial conditions Eqs. (9a) and (9b) the ^1E state is the only initially populated excited state at time = 0 fs. Because of the presence of an energy barrier (of the order of 20 kJ mol^{-1}) at the entrance of the channel leading to the Co–H bond homolysis, the total dissociation of the hydride is prevented. The wave packet breaks into two parts: one part has enough kinetic energy to overcome this barrier and leads to the formation of the H + $Co(CO)_4$ (^1E) primary products ; the other fraction represents intramolecular vibrational energy redistribution (IVR) of the non-dissociative part.

In 20 fs 35% of the system dissociates. Immediately after the initial excitation to the ^1E state, the $^3A_1$ state is weakly populated through intersystem crossing. The small fraction of the wave packet coming from the singlet potential runs out exclusively toward the primary products $H+Co(CO)_4$ ($^3A_1$), directly formed in their electronic ground state. A mechanism of continuous transition-dissociation has been proposed. As the reaction on the $^3A_1$ is fast and total, the reaction probability is equivalent to the $^1E \rightarrow {}^3A_1$ transition probability. Over a duration of 3 ps this probability can be estimated to 9%.

The molecular reaction dynamics of competitive direct dissociation on the ^1E state versus the indirect dissociation via the ^3E state have been simulated on the same way and are illustrated by the time evolution of representative wave packet $\Psi_{^1E}(q_a, q_b, t)$ and $\Psi_{^3E}(q_a, q_b, t)$ on the coupled potentials, left side of Fig. 1(B) and right side of Fig. 1(B), respectively. As far as the ^1E potential is concerned the dynamical events on this state are not different from those accompanying the $^1E \rightarrow {}^3A_1$ transition, namely nontotal and fast breaking of the Co–H bond. The presence of an energy barrier of the order of 72 kJ mol^{-1} at the entrance of the valley corresponding to the Co–H bond homolysis on the ^3E potential does not prevent this primary reaction which leads to $H+Co(CO)_4(^3E)$ products. The probability for observing this reaction reaches 7% in 2 ps whereas the probability for observing $CO+HCo(CO)_3$ (^3E) is quasi nul. The $^1E \rightarrow {}^3E$ intersystem crossing timescale has been estimated at 38 ps.

3.2. Photodissociation dynamics of $H_2Fe(CO)_4$: evidence for competitive primary reactions [22]

The photochemical reactivity of $H_2Fe(CO)_4$

$$H_2Fe(CO)_4 \xrightarrow{h\nu} H_2 + Fe(CO)_4 \quad \text{(R3)}$$

$$H_2Fe(CO)_4 \xrightarrow{?} CO + H_2Fe(CO)_3 \quad \text{(R4)}$$

is described by wave packet propagation on the two-dimensional CASSCF/MR-CCI PES calculated under C_s symmetry constraint along the two reaction coordinates

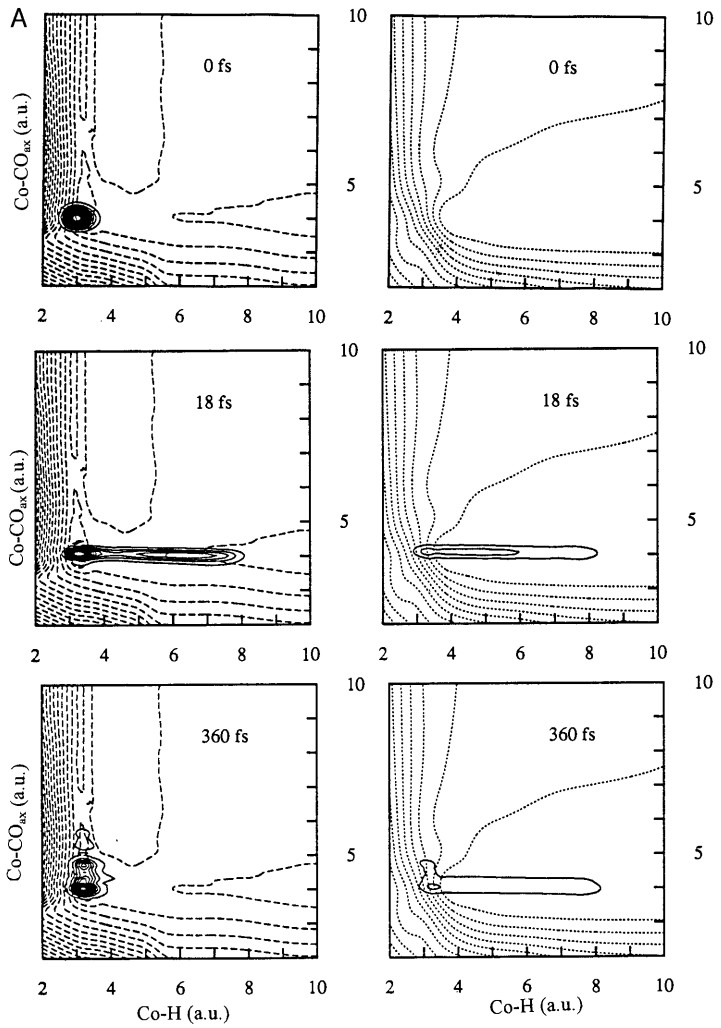

Fig. 1. (A) Time evolution of the $\Psi_{^1E}(q_a, q_b, t)$ wave packet (solid line) on the $V_{^1E}(q_a, q_b)$ potential (dashed line) (left) and $\Psi_{^3A_1}(q_a, q_b, t)$ wave packet (solid line) on the $V_{^3A_1}(q_a, q_b)$ potential (dashed line) (right); (B) Time evolution of the $\Psi_{^1E}(q_a, q_b, t)$ wave packet (solid line) on the $V_{^1E}(q_a, q_b)$ potential (dashed line) (left) and $\Psi_{^3E}(q_a, q_b, t)$ wave packet (solid line) on the $V_{^3E}(q_a, q_b)$ potential (dashed line) (right).

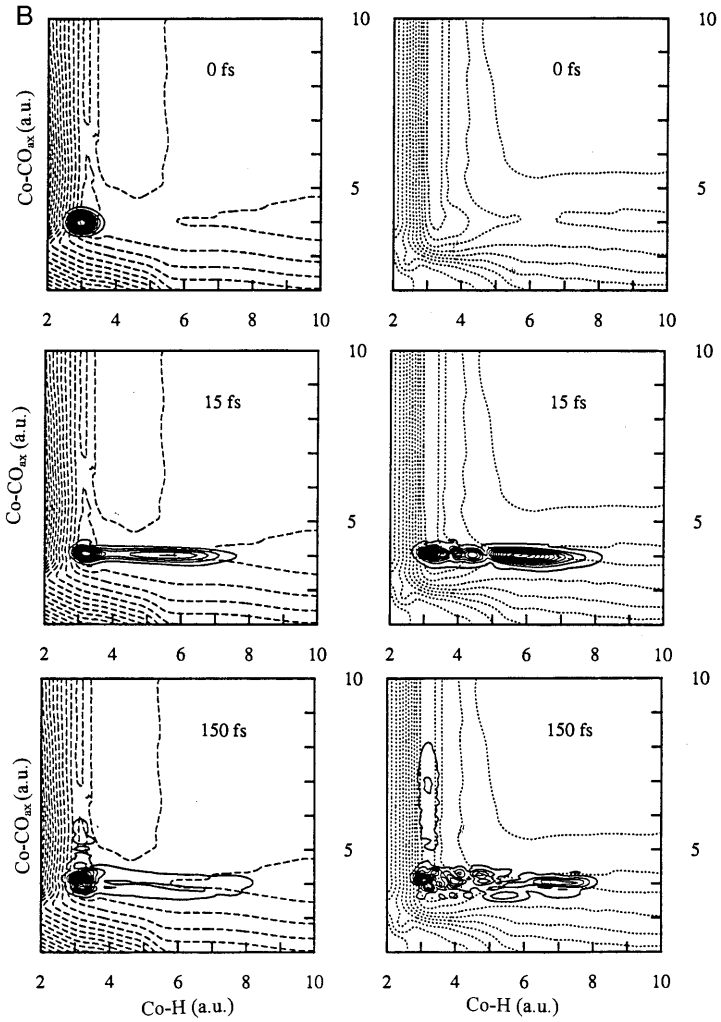

Fig. 1. (*continued*)

$q_a = [Fe–H_2]$ and $q_b = [Fe–CO]$. The photoinduced molecular hydrogen elimination (Eq. (R3)) has been observed in low-temperature matrices [32]. In contrast to $HCo(CO)_4$ no experimental evidence of the occurrence of the CO loss from $H_2Fe(CO)_4$ (R4) has been published. However this primary reaction seems to occur after irradiation of the analog $H_2Os(CO)_4$ [33].

The CASSCF/MR-CCI excitation energies to the lowest singlet excited states of $H_2Fe(CO)_4$ are reported in Table 2. Two allowed transitions, namely $a^1A_1 \rightarrow a^1B_1$ and $a^1A_1 \rightarrow b^1A_1$, present rather large dipole transition moments whereas the $a^1A_1 \rightarrow a^1B_2$ transition corresponding mainly to the $3d_{x^2-y^2} \rightarrow \sigma_u^*$ excitation has a very low dipole transition moment ($\mu = 0.013$ au). These first allowed transitions calculated between 38 000 and 42 000 cm^{-1} range in the energy domain of the experimental absorption spectrum (34 500–41 500 cm^{-1}) [34]. The theoretical absorption spectrum ob-tained after propagation of selected $\Psi_{c^1A'}(q_a, q_b, t)$ and $\Psi_{b^1A'}(q_a, q_b, t)$ wave packets on the $V_{c^1A'}(q_a, q_b)$and $V_{b^1A'}(q_a, q_b)$ potentials associated to the b^1A_1 (c^1A' in C_s symmetry) ($3d_{x^2-y^2} \rightarrow \sigma_g^*$) and a^1B_1 (b^1A' in C_s symmetry) ($3d_{yz} \rightarrow \sigma_g^*$) excited states, respectively is represented in Fig. 2.

The spectrum is characterized by two broad absorption bands without any structure corresponding to the b^1A_1 and a^1B_1 excited states. The a^1B_1 absorption at 36 700 cm^{-1} agrees perfectly with the experimental maximum at 270 nm (37 040 cm^{-1}). The comparison with the experimental spectrum at higher energies is featureless, since the detection is close to the lower limit of the spectrometer. The experimental excitation energy (254 nm or 39 400 cm^{-1}) necessary to induce molecular hydrogen elimination of $H_2Fe(CO)_4$ should populate the b^1A_1 and a^1B_1 excited states. On the basis of preliminary one-dimensional simulations which point to a low efficiency of intersystem crossings and to a minor role of the a^1B_2 state in the photodissociation process [22] the a^1B_2 singlet state and the low-lying triplet excited states have been excluded from the two-dimensional simulation.

The time evolution of representative wave packets $\Psi_{b^1A'}(q_a, q_b, t)$ on the $V_{b^1A'}(q_a, q_b)$ potential originated from the a^1B_1 excited state of $H_2Fe(CO)_4$ is depicted in Fig. 3.

Table 2
CASSCF/MR-CCI excitations energies (cm^{-1}) to the low-lying singlet excited states of $H_2Fe(CO)_4$ and associated dipole transition moments μ (a.u.)

Transition	One-electron excitation in the principal configuration	CASSCF/MR-CCI	μ
$a^1A_1 \rightarrow a^1B_1$	$3d_{yz} \rightarrow \sigma_g^*$	38 500	0.327
$a^1A_1 \rightarrow a^1B_2$	$3d_{x^2-y^2} \rightarrow \sigma_u^*$	39 350	0.013
$a^1A_1 \rightarrow b^1A_1$	$3d_{x^2-y^2} \rightarrow \sigma_g^*$	42 180	0.275
$a^1A_1 \rightarrow b^1B_2$	$\sigma_u \rightarrow \sigma_g^*$	68 667	

After the initial $a^1A_1 \rightarrow a^1B_1$ transition, in a very short time scale (15 fs) the wave packet evolves to the dissociation channel corresponding to H_2 elimination. After 30 fs a splitting of the initial wave packet is observed, the main fraction leading to the primary products $H_2 + Fe(CO)_4$ (b^1A') in 40 fs, the remaining part dissociating to the carbonyl loss primary products in a time scale of the order of 100 fs. The probability of this minor reaction deduced from integration over the whole reaction time reaches 4%. The elimination of molecular hydrogen is the major process overall the absorption region and the probability of this primary reaction increases with the wavelength of irradiation. The ultra-fast (40 fs) and total elimination of H_2 is the only process observed when propagating a representative $\Psi_{c^1A'}(q_a, q_b, t)$ wave packet on the $V_{c^1A'}(q_a, q_b)$ potential originated in the b^1A_1 excited state of $H_2Fe(CO)_4$ [22].

3.3. Photodissociation dynamics and electronic spectroscopy of HM(CO)$_3$(H-DAB) (M = Mn, Re) prototypes for MLCT complexes [23,30,35,36]

The photochemical reactions currently observed after irradiation in the visible (500 nm) of the $LM(CO)_3$(α-diimine) complexes (where L represents a metal fragment or alkyl or halide group and M = Mn or Re) are either the homolytic cleavage of the M–L bond or the carbonyl loss,

$$LM(CO)_3(\alpha\text{-diimine}) \xrightarrow{h\nu} {}^{\bullet}L + {}^{\bullet}M(CO)_3(\alpha\text{-diimine}) \quad (R5)$$

$$LM(CO)_3(\alpha\text{-diimine}) \xrightarrow{h\nu} CO + LM(CO)_2(\alpha\text{-diimine}) \quad (R6)$$

The quantum yields of the primary reactions R5 and R6 depend mainly on the nature of the ligand L and on the metal center. The photoreactivity of the manganese complexes is characterized by a high quantum yield for the CO loss ($0.6 < \phi$ co < 1.0) while the rhenium complexes show exclusively radicals formations (R5) or intense emission. The aim of the theoretical comparative study described below is to understand and to rationalize these different photochemical behaviors.

The CASSCF/MR-CCI excitation energies to the low-lying singlet excited states of $HMn(CO)_3$(H-DAB) and $HRe(CO)_4$(H-DAB) are collected in Tables 3 and 4, respectively, together with their oscillator strengths. For both complexes the visible part of the absorption spectrum consists of three MLCT states corresponding to $d \rightarrow \pi^*_{H\text{-}DAB}$ excitations and ranging between 18 000 and 23 020 cm^{-1} and 15 500 and 22 500 cm^{-1} for M = Mn and M = Re, respectively. The c^1A' ($d_{xz} \rightarrow \pi^*_{H\text{-}DAB}$) state is the only one which has a sufficient oscillator strength ($f = 0.39$ in $HMn(CO)_3$(H-DAB) and 0.38 in $HRe(CO)_3$(H-DAB)) to contribute significantly to the visible absorption. One excited state has been found to contribute mainly to the UV absorption, namely the d^1A' ($\sigma_{M-H} \rightarrow \pi^*_{H\text{-}DAB}$) so-called Sigma-Bond-to-Ligand-Charge-Transfer (SBLCT) state calculated at 35 600 ($f = 0.11$) and 33 490 cm^{-1} ($f = 0.15$) in $HMn(CO)_3$(H-DAB) and HRe(CO)3(H-DAB), re-spectively. The theoretical absorption spectra of the two molecules obtained by propagation of the $\Psi_{b^1A'}(q_a, q_b, t)$, $\Psi_{c^1A'}(q_a, q_b, t)$ and $\Psi_{d^1A'}(q_a, q_b, t)$ wave packets on the corresponding two-dimensional PES calculated as a function of $q_a = [M–H]$ and $q_b = [M–CO_{ax}]$ with the following initial conditions

$$\Psi_{b^1A'}(q_a, q_b, t = 0) = \mu_{a^1A' \rightarrow b^1A'} \Phi_{a^1A',0,0}(q_a, q_b) \quad (10a)$$

$$\Psi_{c^1A'}(q_a, q_b, t = 0) = \mu_{a^1A' \rightarrow c^1A'} \Phi_{a^1A',0,0}(q_a, q_b) \quad (10b)$$

$$\Psi_{d^1A'}(q_a, q_b, t = 0) = \mu_{a^1A' \rightarrow d^1A'} \Phi_{a^1A',0,0}(q_a, q_b) \quad (10c)$$

are shown in Fig. 4(a,b), respectively,

These spectra reproduce the main features of the experimental spectra reported for this class of molecules, namely an intense absorption band around 500 nm (20 000 cm^{-1}) and a shoulder in the UV energy domain.

The photodissociation dynamics of $HMn(CO)_3$(H-DAB) after absorption in the visible have been followed

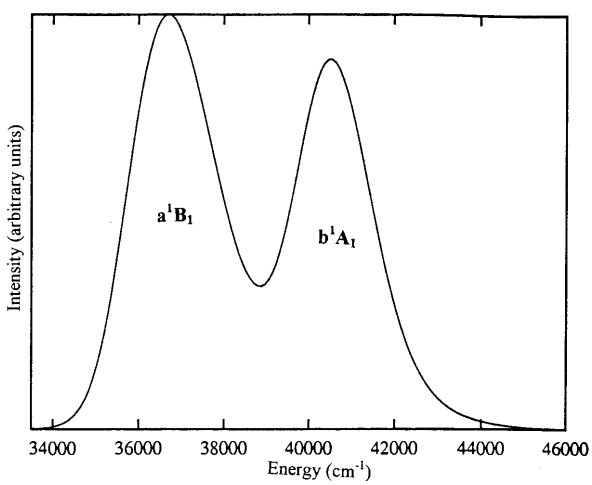

Fig. 2. Simulated absorption spectrum of $H_2Fe(CO)_4$.

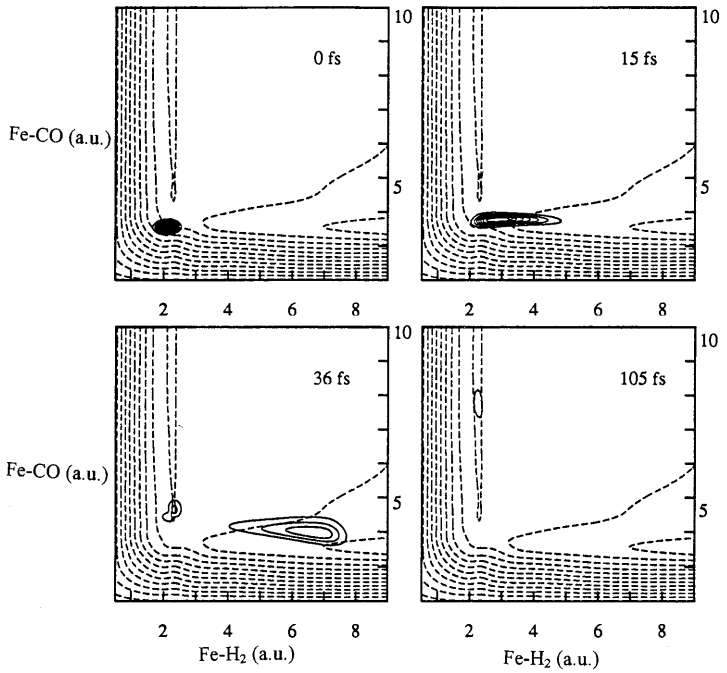

Fig. 3. Time evolution of the $\Psi_{b^1A'}(q_a, q_b, t)$ wave packet (solid line) on the $V_{b^1A'}(q_a, q_b)$ potential (dashed line) originated from the a^1B_1 excited state of $H_2Fe(CO)_4$.

Table 3
CASSCF/MR-CCI excitations energies (in cm^{-1}) to the low-lying singlet excited states of $HMn(CO)_3$(H-DAB) and associated oscillator strengths f

Transition	One-electron excitation in the principal configuration	CASSCF/MR-CCI	f
$a^1A' \rightarrow a^1A''$	$3d_{yz} \rightarrow \pi^*_{H\text{-}DAB}$	18 000	0.04
$a^1A' \rightarrow b^1A'$	$3d_{x^2-y^2} \rightarrow \pi^*_{H\text{-}DAB}$	21 060	0.03
$a^1A' \rightarrow c^1A'$	$3d_{xz} \rightarrow \pi^*_{H\text{-}DAB}$	23 020	0.39
$a^1A' \rightarrow d^1A'$	$\sigma_{Mn-H} \rightarrow \pi^*_{H\text{-}DAB}$	35 600	0.11
$a^1A' \rightarrow d^3A'$ [a]	$\sigma_{Mn-H} \rightarrow \pi^*_{H\text{-}DAB}$	68 667	

[a] ^{3}SBLCT (d^3A') state dissociative for the Mn–H bond homolysis. Spin–orbit coupling with the ^{1}MLCT (c^1A') state: 75 cm^{-1}.

Table 4
CASSCF/MR-CCI excitations energies (in cm^{-1}) to the low-lying singlet excited states of $HRe(CO)_3$(H-DAB) and associated oscillator strengths f

Transition	One-electron excitation in the principal configuration	CASSCF/MR-CCI	f
$a^1A' \rightarrow a^1A''$	$5d_{yz} \rightarrow \pi^*_{H\text{-}DAB}$	15 500	0.0
$a^1A' \rightarrow b^1A'$	$5d_{x^2-y^2} \rightarrow \pi^*_{H\text{-}DAB}$	17 400	0.0
$a^1A' \rightarrow c^1A'$	$5d_{xz} \rightarrow \pi^*_{H\text{-}DAB}$	22 500	0.38
$a^1A' \rightarrow d^1A'$	$\sigma_{Mn-H} \rightarrow \pi^*_{H\text{-}DAB}$	33 500	0.15
$a^1A' \rightarrow d^3A'$ [a]	$\sigma_{Mn-H} \rightarrow \pi^*_{H\text{-}DAB}$	30 420	

[a] ^{3}SBLCT (d^3A') state dissociative for the Re–H bond homolysis. Spin–orbit coupling with the ^{1}MLCT (c^1A') state: 315 cm^{-1}.

by propagation of the $\Psi_{b^1A'}(q_a, q_b, t)$ and $\Psi_{c^1A'}(q_a, q_b, t)$ wave packets on the non-adiabatically coupled $V_{b^1A'}(q_a, q_b)$ and $V_{c^1A'}(q_a, q_b)$ potentials (Fig. 5).

After $a^1A' \rightarrow c^1A'$ initial transition the wave packet evolves in a very short time scale (< 100 fs) to the dissociation channel corresponding to the axial CO loss. The dissociation probability reaches 99% in 400 fs. This direct and ultra-fast channel of deactivation of $HMn(CO)_3$(H-DAB) is the only primary reaction ob-served after irradiation of the molecule in the visible energy domain. Indeed the ^{1}MLCT potentials are quasi-bound and present energy barriers at the entrance of the channel corresponding to the Mn–H bond homolysis preventing the occurrence of this primary reaction [8c]. The role of the d^3A' ($\sigma_{Mn-H} \rightarrow \pi^*_{H\text{-}DAB}$) so-called SBLCT which is dissociative for the Mn–H bond homolysis

reaction [8c] is minor in this first row transition metal complex in which the low-lying singlet MLCT states are dissociative with respect to the CO loss. The spin–orbit interaction between the ^{3}SBLCT (d^3A') state and the ^{1}MLCT (c^1A') state initially populated has been evaluated to 75 cm^{-1} in the Franck–Condon region [35] (see Table 3) and never exceeds a few tens of wavenumbers along the Mn–H bond homolysis pathway. On the basis of preliminary one-dimensional simulations including nine non-adiabatically and spin–orbit coupled potentials among them the low-lying triplet states [23] it has been shown that indirect Mn–H bond homolytic cleavage via the ^{3}SBLCT through $^1\text{MLCT} \rightarrow {}^3\text{SBLCT}$ intersystem crossing has a negligible probability close to 0 and is not competitive with the ultra-fast and total dissociation of the CO ligand via the ^{1}MLCT state.

In contrast the PES associated to the low-lying excited states of $HRe(CO)_3$(H-DAB) [36] are quasi-bound in both directions in agreement with a low photoreactivity. The time evolution of representative $\Psi_{c^1A'}(q_a, q_b, t)$ and $\Psi_{d^3A'}(q_a, q_b, t)$ wave packets on the spin–orbit coupled $V_{c^1A'}(q_a, q_b)$ and $V_{d^3A'}(q_a, q_b)$ potentials associated to the ^{1}MLCT state populated after visible irradiation and to the ^{3}SBLCT state, respectively is represented in Fig. 6.

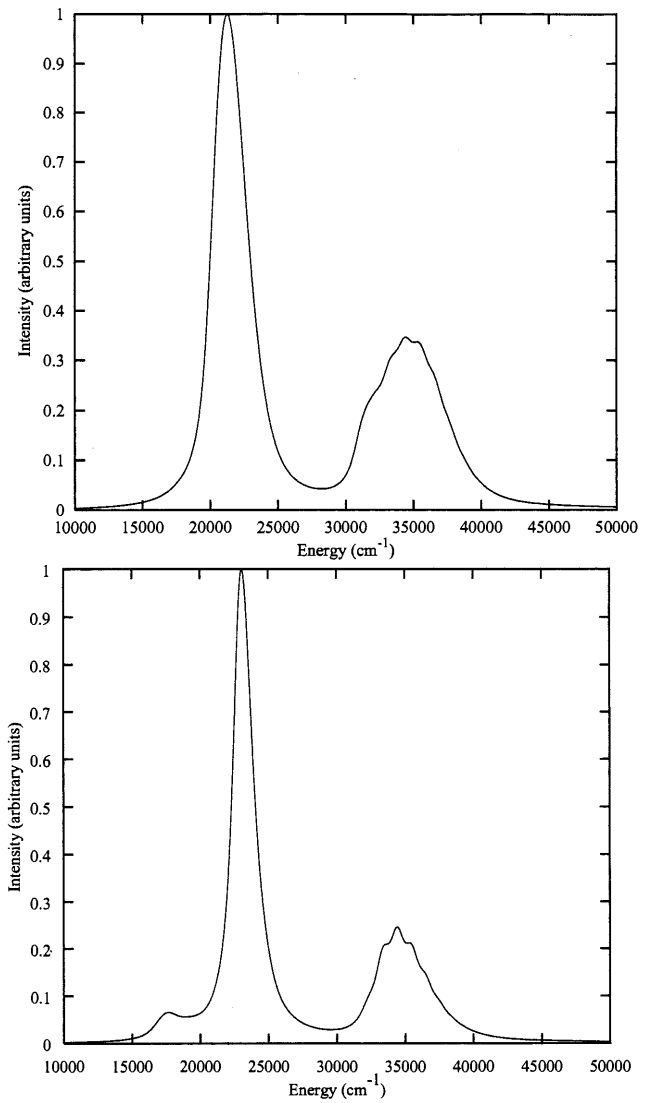

Fig. 4. (a) Theoretical absorption spectrum of $HMn(CO)_3$(H-DAB) and (b) of $HRe(CO)_3$(H-DAB).

The spin–orbit coupling between the ^{1}MLCT (c^1A') state and the dissociative ^{3}SBLCT (d^3A') state of $HRe(CO)_3$(H-DAB) has a value of 315 cm^{-1} (Table 4) at equilibrium geometry. This is four times the value obtained for the manganese complex. The molecular dynamics has been followed solving a set of coupled time-dependent Schrödinger equations

$$i\hbar \frac{\partial}{\partial t} \Psi_{c^1A'}(q_a, q_b, t) = [T_{nu} + V_{c^1A'}]\Psi_{c^1A'}(q_a, q_b, t) + V_{c^1A'd^3A'}\Psi_{d^3A'}(q_a, q_b, t) \quad (11a)$$

$$i\hbar \frac{\partial}{\partial t} \Psi_{d^3A'}(q_a, q_b, t) = [T_{nu} + V_{d^3A'}]\Psi_{d^3A'}(q_a, q_b, t) + V_{d^3A'c^1A'}\Psi_{c^1A'}(q_a, q_b, t) \quad (11b)$$

with the following initial conditions

$$\Psi_{c^1A'}(q_a, q_b, t = 0) = \mu_{a^1A' \rightarrow c^1A'}\Phi_{a^1A',0,0}(q_a, q_b) \quad (12a)$$

$$\Psi_{d^3A'}(q_a, q_b, t = 0) = 0 \quad (12b)$$

and the spin–orbit coupling terms given in [35].

The ultra-fast and total photodissociation of $HRe(CO)_3$(H-DAB) is prevented on one side by the presence of energy barriers at the entrance of the Re–H bond homolysis channel and on the other side by attractive potentials (CO loss dissociation pathway). As a consequence illustrated in Fig. 6 (left side) the main part of the initial wave packet gets trapped in the potential well of the ^{1}MLCT (c^1A') excited state where it starts an oscillating motion. However, immediately after the initial excitation the ^{3}SBLCT (d^3A') state is weakly populated through intersystem crossing (right side of Fig. 6). The small fraction of the wave packet coming from the singlet potential runs out exclusively toward the primary products H + $Re(CO)_3$(H-DAB) in their ground state (right side of Fig. 6). The mechanism of continuous transition/dissociation is very similar to the one proposed for $HCo(CO)_4$. The probability of dissociation is very low and is estimated to 1% after 1 ps of simulation.

4. Conclusions

The photodissociation dynamics of four transition metal hydride complexes, $HCo(CO)_4$, $H_2Fe(CO)_4$ representative of mono and di-hydrides carbonyls and $HM(CO)_3$(H-DAB) (M = Mn, Re) model systems for Metal-to-Ligand-Charge-Transfer complexes have been reported.

The efficiency of concurrent photochemical reactions, metal–hydrogen bond homolysis or molecular hydro-

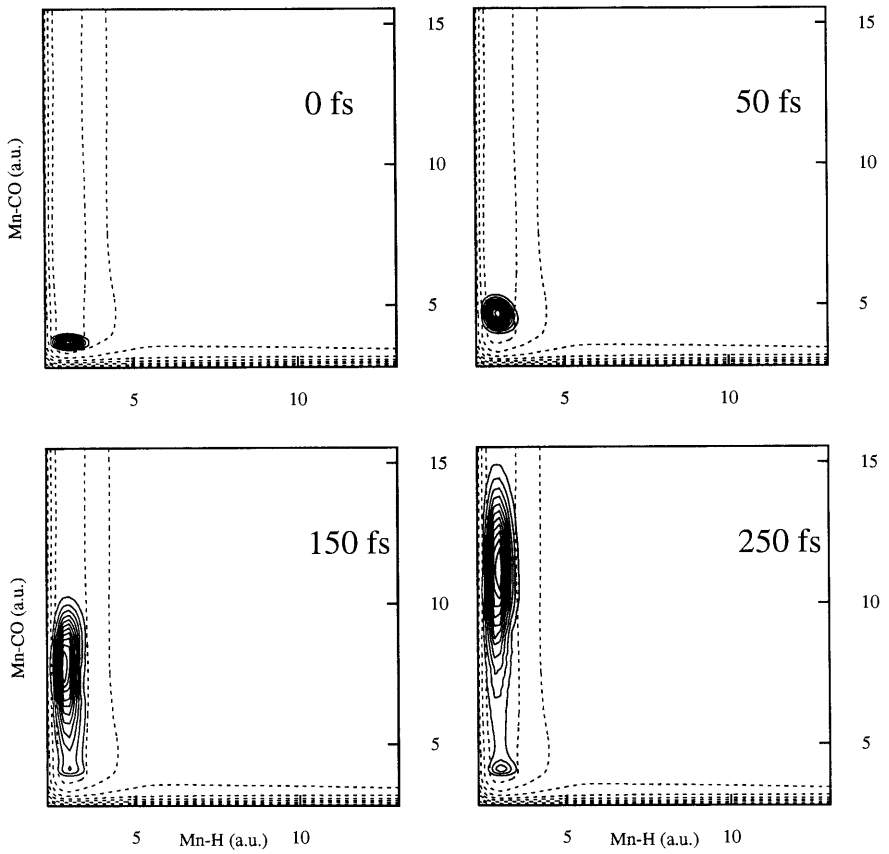

Fig. 5. Time evolution of the $\Psi_{c1A'}(q_a, q_b, t)$ wave packet (solid line) on the $V_{c1A'}(q_a, q_b)$ potential (dashed line) of $HMn(CO)_3$(H-DAB).

gen elimination versus carbonyls loss, occurring after irradiation in the UV absorption domain ($HCo(CO)_4$ or $H_2Fe(CO)_4$) or in the visible ($HM(CO)_3$(H-DAB)) depends on the hierarchy in time of the elementary events occurring between the initial absorption and the formation of the primary products detected experimentally.

The shape of the potential associated to the singlet excited state initially populated will control entirely the future of the molecule in the first hundred of femtoseconds. In the case of dissociative potentials ultra-fast and total dissociation will occur in a few tens of femtoseconds (for the M–H bond breaking) or a few hundreds of femtoseconds (for the CO loss). Other indirect and slower dissociative processes via intersystem crossing, internal conversions or via channels possessing energy barriers along their reaction pathways are not competitive with this efficient direct dissociation. The efficiency of intersystem crossing processes leading most of the time to indirect dissociation via low-lying triplet states corresponding to a $\sigma_{M-H} \rightarrow \sigma^*_{M-H}$ excitation, depends mainly on the relative position of the potentials associated to the populated singlet and to the dissociative triplet. The presence of a crossing between these two states in the Franck–Condon region will enhance the probability of indirect dissociation via the triplet state which will occur in ten of picoseconds time- scale. The spin–orbit interaction does not increase significantly the efficiency of the radiationless transition as it has been observed in $HRe(CO)_3$(H-DAB). Indeed despite of a spin–orbit interaction of a few hundred of wavenumbers the unfavorable position of the singlet-triplet crossing makes the indirect Re–H bond homolysis via the ^{3}SBLCT state very slow and not total. The control of the photodissociation dynamics at the early stage by the shape of the potential associated to the singlet absorbing state is well illustrated by the comparison between the two MLCT complexes $HMn(CO)_3$(H-DAB) and $HRe(CO)_3$(H-DAB) which differ only by their metal center (first-row transition metal hydride versus third-row transition metal hydride). In the manganese complex the potential associated to the ^{1}MLCT absorbing state is dissociative for the CO loss and this reaction is ultra-fast and total whereas in the rhenium complex the quasi-bound shape of this potential in this direction prevents the occurrence of this fast primary reaction. The difference between the two complexes is mainly due to the dπ–pπ back donation at the level of the metal–CO_{axial} bond, which is more important in first-row transition metal carbonyls than in third-row analogs. This is illustrated experimentally by the shift of the lowest IR band observed when going from the Mn to the Re complexes ($\nu(CO_{axial}) = 1900$ cm^{-1} for $Mn(Me)(CO)_3$(i-PrDAB) [37] versus $\nu(CO_{axial}) = 1888$ cm^{-1} for $Re(Me)(CO)_3$(i-PrDAB) [38] in THF). Consequently, the excitation from the metal center to the π^* acceptor orbital of the α-diimine ligand which reduces

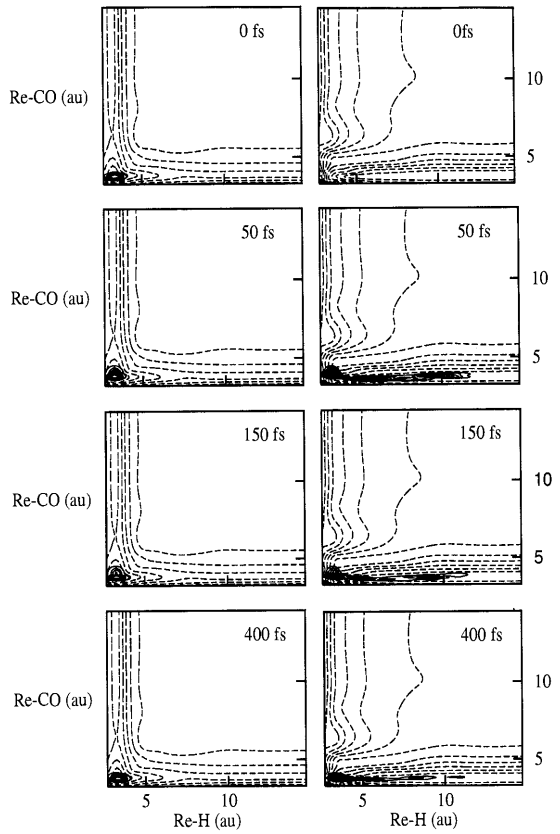

Fig. 6. Time evolution of the $\Psi_{c^1A'}(q_a, q_b, t)$ wave packet (solid line) on the $V_{c^1A'}(q_a, q_b)$ potential (dashed line) (left) and $\Psi_{d^3A'}(q_a, q_b, t)$ wave packet (solid line) on the $V_{d^3A'}(q_a, q_b)$ potential (dashed line) (right) of $HRe(CO)_3$(H-DAB).

this bonding interaction in the MLCT states is responsible for the weakening of the $Mn–CO_{axial}$ bond.

When the potential presents wells and more or less high energy barriers in one or several channels the behavior of the system in the first femtoseconds is more complicated to analyze. Indeed, splitting of the original wave packets in bound and dissociative parts can be observed leading either to two primary products like in $H_2Fe(CO)_4$ ($H_2 + Fe(CO)_4$ or $CO + H_2Fe(CO)_3$) via a single excited state or to one primary product via two different excited states like in $HCo(CO)_4$ ($H + Co(CO)_4(^1E)$ and $^3A_1$).

Further work, which has to be performed in connection with femtosecond laser pump and probe experiments should be oriented towards the laser driven photodissociation of transition metal hydrides.

References

[1] (a) N.W. Hoffman, T.L. Brown, Inorg. Chem. 17 (1978) 613. (b) P. Grebenik, A.J. Downs, M.L.H. Green, R.N. Perutz, J. Chem. Soc. Chem. Commun. (1979) 742.
[2] (a) A.J. Rest, J.J. Turner, J. Chem. Soc. Chem. Commun. (1969) 375. (b) B.H. Beyers, T.L. Brown, J. Am. Chem. Soc. 99 (1977) 2527. (c) G.L. Geoffroy, M.G. Bradley, Inorg. Chem. 16 (1977) 744.
[3] (a) G.L. Geoffroy, Prog. Inorg. Chem. 27 (1980) 123. (b) A.H. Janowiz, R.G. Bergman, J. Am. Chem. Soc. 104 (1982) 352. (c) T.L. Wenzel, R.G. Bergman, J. Am. Chem. Soc. 108 (1986) 4856. (d) I. Wu, R.G. Bergman, J. Am. Chem. Soc. 111 (1989) 7628.
[4] (a) C. Daniel, A. Veillard, in: A. Dedieu (Ed.), Transition Metal Hydrides, VCH, New York, 1991, pp. 235–261 and references therein. (b) A. Veillard, Chem. Phys. Lett. 170 (1990) 441.
[5] (a) C. Daniel, I. Hyla-Kryspin, J. Demuynck, A. Veillard, New J. Chem. 9581 (1985). (b) A. Veillard, A. Strich, J. Am. Chem. Soc. 110 (1998) 3793.
[6] A. Veillard, C. Daniel, A. Strich, Pure Appl. Chem. 52 (1988) 215.
[7] C. Daniel, J. Phys. Chem. 95 (1991) 2394.
[8] (a) C. Daniel, Coord. Chem. Rev. 97 (1990) 141. (b) C. Daniel, J. Am. Chem. Soc. 114 (1992) 1625. (c) K. Finger, C. Daniel, J. Am. Chem. Soc. 117 (1995) 12 322.
[9] R. Schinke, in: Photodissociation Dynamics, Cambridge University Press, Cambridge, 1993, and references therein.
[10] D.G. Imre, J. Zhang, J. Chem. Phys. 139 (1989) 89.
[11] (a) C. Daniel, E. Kolba, L. Lehr, T. Schröder, J. Manz, J. Phys. Chem. 98 (1994) 9823. (b) C. Daniel, R. de Vivie-Riedle, M.C. Heitz, J. Manz, P. Saalfrank, Int. J. Quant. Chem. 57 (1996) 595.
[12] A.H. Zewail, Femtochemistry, vol. 1–2, World Scientific, Singapore, 1994, and references therein.
[13] J. Manz, L. Wöste, Femtosecond Chemistry, VCH, Weinheim, 1995.
[14] S.K. Kim, S. Pedersen, A.H. Zewail, Chem. Phys. Lett. 233 (1995) 500.
[15] (a) L. Banares, T. Baumert, M. Bergt, B. Kiefer, G. Gerber, Chem. Phys. Lett. 267 (1997) 141. (b) L. Banares, T. Baumert, M. Bergt, B. Kiefer, G. Gerber, J. Chem. Phys. 108 (1998) 5799.
[16] S.A. Trushin, W. Fuss, W.E. Schmidt, K.L. Kompa, J. Phys. Chem. A 102 (1998) 4128.
[17] I.R. Farrell, P. Matousek, A. Vlcek Jr., J. Am. Chem. Soc. 121 (1999) 5296.
[18] (a) D.J. Stufkens, Comments Inorg. Chem. 13 (1992) 359. (b) D.J. Stufkens, Coord. Chem. Rev. 104 (1990) 39.
[19] (a) D. Guillaumont, C. Daniel, Chem. Phys. Lett. 257 (1996) 1. (b) I. Cote-Bruand, C. Daniel, to be submitted.
[20] C. Daniel, M.C. Heitz, J. Manz, C. Ribbing, J. Chem. Phys. 102 (1995) 905.
[21] M.C. Heitz, C. Ribbing, C. Daniel, J. Chem. Phys. 106 (1997) 1421.
[22] M.C. Heitz, C. Daniel, J. Am. Chem. Soc. 119 (1997) 8269.
[23] (a) D. Guillaumont, C. Daniel, J. Am. Chem. Soc. 121 (1999) 11 733. (b) D. Guillaumont, C. Daniel, Coord. Chem. Rev. 177 (1998) 181.
[24] (a) B. Hartke, J. Manz, J. Mathis, J. Chem. Phys. 139 (1989) 123. (b) T. Joseph, T.M. Kruel, J. Manz, I. Rexrodt, J. Chem. Phys. 139 (1989) 323.
[25] R. Kossloff, H. Tal-Ezer, Chem. Phys. Lett. 127 (1986) 223.
[26] A. Askar, A.S. Cakmak, J. Chem. Phys. 68 (1978) 2794.
[27] (a) H. Tal-Ezer, R. Kosloff, J. Chem. Phys. (b) J. Chem. Phys. 81 (1984) 3967.
[28] G. Katz, R. Baer, R. Kosloff, Chem. Phys. Lett. 239 (1995) 230.
[29] (a) R.L. Sweany, Inorg. Chem. 19 (1980) 3512. (b) R.L. Sweany, Inorg. Chem. 21 (1982) 752. (c) R.L. Sweany, J. Am. Chem. Soc. 104 (1982) 3739.
[30] K. Finger, C. Daniel, P. Saalfrank, B. Schmidt, J. Phys. Chem. 100 (1996) 3368.
[31] C. Ribbing, C. Daniel, J. Chem. Phys. 100 (1994) 6591.
[32] R.L. Sweany, J. Am. Chem. Soc. 103 (1981) 2410.
[33] A.J. Rest, unpublished work cited by J. Evans, J.R. Norton, J. Am. Chem. Soc. 96 (1974) 7577.
[34] R.L. Sweany, in: A. Dedieu (Ed.), Transition Metal Hydrides, VCH, New York, 1991, pp. 65–101.
[35] C. Daniel, D. Guillaumont, C. Ribbing, B. Minaev, J . Phys. Chem. A 103 (1999) 5766.
[36] I. Cote-Bruand, C. Daniel, submitted for publication.
[37] (a) B.D. Rossenaar, E. Lindsay, D.J. Stufkens, A. Vlcek Jr, Inorg. Chim. Acta 250 (1996) 5. (b) B.D. Rossenaar, D.J. Stufkens, A. Oskam, J. Fraanje, K. Goubitz, Inorg. Chim. Acta 247 (1996) 215.
[38] B.D. Rossenaar, F. Hartl, D.J. Stufkens, Inorg. Chem. 35 (1996) 6194.